An efficient numerical method for uncertainty quantification in cardiology models

Xindan Gao*[1], Wenjun Ying†[2], and Zhiwen Zhang‡[3]

[1,2]School of Mathematical sciences, Shanghai Jiao Tong University, 800 Dongchuan Road, Minhang, Shanghai, P.R. China, 200240.

[3]Department of Mathematics, The University of Hong Kong, Pokfulam Road, Hong Kong.

Abstract

Mathematical models of cardiology involve conductivity and massive parameters describing the dynamics of ionic channels. The conductivity is space dependent and cannot be measured directly. The dynamics of ionic channels are highly nonlinear and the parameters have unavoidable uncertainties since they are estimated using repeated experimental data. Such uncertainties can impact model dependability and credibility since they spread to model parameters during model calibration. It is necessary to study how the uncertainties influence the solution compared to the deterministic solution and to quantify the difference resulting from uncertainty. In this paper, the generalized polynomial chaos method and stochastic collocation method are used to solve the corresponding stochastic partial differential equations. Numerical results are shown to demonstrate that each parameter has different effects on the model responses. More importantly, a quadratic convergence of the expectation is exhibited in the numerical results. The amplitude of standard variance of the stochastic solution can be controlled by the parameter uncertainty. More precisely, the standard variance of the stochastic solution is positively linear to the standard variance of the random parameter. We utilized mono-domain equations which are representative mathematical models to demonstrate the results with the most widely used ionic models Hodgkin-Huxley model and Fitz-Hugh Nagumo model.

KEY WORDS: Computational cardiology, Uncertainty quantification, Generalized polynomial chaos, Hodgkin-Huxley model, Fitz-Hugh Nagumo model.

1 INTRODUCTION

Mathematical models of the Cardiac electro-physiology are important applications in biology. A particularly large volume of researchers has been working on the deterministic models [11, 21, 26]. Owing to advances in both numerical methods and computer hardware, the accuracy and efficiency

*gaoxindan@sjtu.edu.cn
†wying@sjtu.edu.cn
‡zhangzw@hku.hk, corresponding author

of the simulating algorithms have been developed to a high level. The models as well as are developed highly detailed [6]. However, there are still many obstacles applying the simulation results to practical problems since there are different types of variability exist in the mathematical models. For example, ionic channels in cardiac tissue are extremely diverse. Its dynamics are studied from the experimental data of the real cardiac cells with inevitable variability. There are also measurement errors arising from experiments. Except for cell level's variability, the conductivity of the tissue cannot be directly measured easily and accurately neither. Moreover, there may exist intrinsic variability to make the process be stochastic. The papers [10, 14] exhibit several sources of uncertainty in a mathematical model of a real system. With all the sources of uncertainty in cardiac problems, this work gives explorative analysis on how the uncertainties influence the deterministic solutions.

For uncertainty analysis, Monte Carlo sampling (MCS) is one of the most commonly used method. MCS is very powerful and flexible and can be easily extended to a complex system as long as there is a well-established solver for the corresponding deterministic system. But the statistical quantities of the solution converge relatively slowly, *e.g.*, the mean value converges at the rate of $\frac{1}{\sqrt{N}}$, where N is the number of realizations. A large number of realizations should be simulated to get a satisfied accuracy which will involve huge computational cost. However, the expensiveness of cardiac simulation is a well-known difficulty. To get rid of this difficulty, the stochastic collocation method (SC) is a good choice to improve the convergence compared to the MCS [1, 13].

In this paper, we will use the generalized polynomial chaos (gPC) which was recently developed [25, 24, 23, 16]. The original polynomial chaos (PC) method was first proposed by Wiener [22] and in [8] the stochastic finite elements method was proposed to elliptic PDEs parametrized by Gaussian random variables. The gPC employs different types of the orthogonal polynomial chaos of the input random parameters including Hermite polynomial chaos as a subset. A gPC expansion is a spectral representation in random space and converges fast if the expanded function is smooth about the random parameters. By using stochastic Garlerkin (SG) procedures to minimize the error of the finite-order gPC expansion, we can solve the deterministic systems transformed from the stochastic equations. To make sure the correctness of the numerical results, we also show the results of SC method for comparison in this work.

Dynamically bi-orthogonal method [4, 5] is an effective tool to solve the time-dependent stochastic partial differential equations which construct the sparsest representation of the stochastic solution via a bi-orthogonal basis. This method explores the inherent low-dimensional structure of the stochastic solution and tracks the Karhunen-Loeve expansion dynamically. When the expansion order is high, we can choose the dynamically bi-orthogonal method to save considerable computational cost. We remark that similar ideas were proposed in the literature to solve SPDEs efficiently [17, 15]. Some recent developments in high order numerical methods for SPDEs were reviewed in [19].

For uncertainty analysis for cardiac problems, some researchers used sensitivity analysis (SA) method to evaluate the contribution of each parameter to the outputs by plotting the mean effects and calculating the main effect [2, 3, 10]. So far, these papers focus on the uncertainties in ion channel and action potential model parameters, *i.e.*, cell models. While we consider the uncertainties of tissue level as well as the parameters of cell models, the parameters are randomized based on the original values to observe the effects of randomization. The mean value of the parameter is set to be the same as the default value while the standard variance (std) of the parameter is changing within a certain range. We then choose mono-domain equations as the mathematical model and simulation

of mono-domain equations is very heuristic. The difference between the original solution and the stochastic solution is a random variable. So we can observe the statistic quantities of the difference, *e.g.*, the expectation and the standard variance.

An outline of this paper is as follows. In section 2, we will give the description of mono-domain equation and randomization of parameters. In section 3, we will give the general procedure of gPC and the solution procedure of mono-domain equations. In section 4, we will show the numerical results that the expectations of the differences between deterministic solutions and stochastic solutions are quadratically proportional to the standard variance of the random perturbation. And the standard variances of the differences are linearly proportional to the standard variance of the random perturbation. In section 5, some conclusions are given.

2 GOVERNING EQUATION

For the simplicity of exposition, we first introduce a general form of the differential equations modeling the electrical activity of the heart. As stated, a typical mono-domain model consists of a system of singularly perturbed reaction-diffusion equations coupled with a set of stiff nonlinear ordinary differential equations, which read:

$$\begin{aligned} C\frac{\partial v}{\partial t} &= \frac{1}{\rho}\nabla\cdot(k\nabla v) - I_{\text{ion}}(v,\mathbf{q}), x\in D, t\in[0,T], \\ \frac{\partial \mathbf{q}}{\partial t} &= \mathcal{M}(v,\mathbf{q}), x\in D, t\in[0,T]. \end{aligned} \tag{1}$$

with suitable boundary and initial conditions. Here, $D\subset R^d$ represents the computational domain; x is the space variable; t is the time variable; v is a cardiac potential; $\mathbf{q}$ represents the gating variables; C is the membrane capacitance matrix; ρ is the surface to volume ratio of the cardiac cells; k is the spatially dependent conductivity tensor; $I_{\text{ion}}(v,\mathbf{q})$ and $\mathcal{M}(v,\mathbf{q})$ are nonlinear functions, describing the cardiac membrane dynamics.

In effect, the complicated phenomenon of cardiac excitation is essentially determined by the membrane dynamics (property) I_{ion} and $\mathcal{M}$. In this paper, we consider two representative models. One representative model is the Hodgkin-Huxley (HH) model, which is the first membrane model for the nerve action potentials [9]. In the model, there are three gating variables $\mathbf{q}=(q_1,q_2,q_3)^T\in R^3$. The dynamics corresponding to each state variable q_j has the same structure as the following:

$$\frac{\partial q_j}{\partial t} = \alpha_j(v)(1-q_j) - \beta_j(v)q_j,$$

where $\alpha_j(v)$, $\beta_j(v) > 0$ and $0 < q_j < 1$. Here, $\alpha_j(v)$ and $\beta_j(v)$ are nonlinear functions of the transmembrane potential v. The membrane dynamics are given by

$$I_{\text{ion}}(v,\mathbf{q}) = \bar{g}_{\text{Na}}q_1^3q_2(v-E_{\text{Na}}) + \bar{g}_{\text{K}}q_3^4(v-E_{\text{K}}) + g_{\text{leak}}(v-E_{\text{leak}})$$

For a detailed description of the nonlinear dynamics of the Hodgkin-Huxley model, refer to the original paper [9]. Many membrane models of Hodgkin-Huxley type for cardiac action potentials are becoming more and more complex due to the advanced experimental data over years. So the HH model is very representative of this subject.

Another model is a simple and widely used FitzHugh-Nagumo (FHN) model, which has only one

gating variable. The FHN model is given as follows:

$$I_{\text{ion}}(v,q) = -\lambda(q - v(v-\theta)(1-v)),$$

$$\mathcal{M}(v,q) = \alpha v - \beta q.$$

There are some restrictions on the parameters for the deterministic model [20]. For example, the eigenvalue parameter $|\lambda| \gg 1$ is negative. The threshold parameter $\theta \in (0, \frac{1}{2})$, the other two parameters α, β are positive constants such that $\beta = O(1)$ and $\alpha > \frac{1}{4}\beta(1-\theta)^2$. This inequality guarantees that the only stationary state of the reaction in the limit of vanishing diffusion is $(v,q) = (0,0)$ and the traveling wave has positive speed.

Taking the mono-domain equations with FHN model as an example, we give the elemental annotation for this work. Based on the deterministic model, we set the random parameters by giving the deterministic parameters a random perturbation. To distinguish whether the parameters are randomly perturbed, we set the random parameters are as follows:

$$\begin{aligned} k &= \bar{k} + \epsilon_k(x) \\ \lambda &= \bar{\lambda} + \epsilon_\lambda \\ \theta &= \bar{\theta} + \epsilon_\theta \\ \alpha &= \bar{\alpha} + \epsilon_\alpha \\ \beta &= \bar{\beta} + \epsilon_\beta \\ v(x,0) &= \bar{v}(x,0) + \epsilon_v(x) \end{aligned} \tag{2}$$

where $\epsilon_z = c_z\bar{z}$, $z = \lambda, \theta, \alpha, \beta, v$ are random perturbations to each parameter z. And the deterministic parameters are represented by $\bar{k}$, $\bar{\lambda}$, $\bar{\theta}$, $\bar{\alpha}$, $\bar{\beta}$, $\bar{v}(x,0)$. Especially, $\epsilon_k = c_k\bar{k}p(x)$ which means the perturbation of conductivity tensor k is related to the space variables. We should notice that $z = v$ particularly means the initial condition of v has a random perturbation. Set $v(x,t;c_z)$ be the solution of the stochastic partial differential equations (Spde) with parameter z being perturbed. The expectation of the random perturbation c_z is zero , *i.e.*, $\mathbb{E}[c_z] = 0$. Like many other researchers, we consider the random perturbation is uniformly distributed [2, 3, 10].

Notice that the conductivity tensor k in the cardiac problem depends on the spatial variable x. Actually, it is closely related to the rotational anisotropy and inhomogeneity of electrical conductivities [7], the microscopic structure as well as the fiber orientation of the cardiac tissue. In practice, however, scientists never have access to all this information. Thus, we set the perturbation of the conductivity tensor k is related to the space variables. In this paper, we set the perturbation of k in two dimensions is

$$\epsilon_k = c_k\bar{k}\sin(\pi(x_1 + x_2)). \tag{3}$$

Here c_k is a uniformly random variable. Meanwhile the parameters in I_{ion} and $\mathcal{M}$ are generated by plenty of repeated experiments. So, there exit unavoidable measurement errors in experiments. In this paper, we only consider the case that those cell model parameters are not related to the space variables, *i.e.*,

$$\epsilon_z = c_z\bar{z}, \quad z = \lambda, \theta, \alpha, \beta, v, \tag{4}$$

where c_z are random variables.

3 SOLUTION PROCEDURE

The generalized polynomial chaos (gPC) or the Wiener-Askey chaos expansion employs more orthogonal polynomials from Askey scheme including the classical Hermite polynomial chaos. The gPC expansion basis represents general non-Gaussian processes more efficiently. A general second-order random process $X(\omega)$ can be represented by gPC as follows

$$X(\omega) = \sum_{i=0}^{\infty} a_i H_i(\boldsymbol{\xi}(\omega)), \tag{5}$$

where $\boldsymbol{\xi}$ is a multi-dimensional random variable. Let Wiener-Askey polynomials $\{H_i(\boldsymbol{\xi})\}$ denote the one-dimensional, $W(\boldsymbol{\xi})$-orthogonal polynomials, *i.e.*,

$$\int H_i(\boldsymbol{\xi}) H_j(\boldsymbol{\xi}) W(\boldsymbol{\xi}) d\boldsymbol{\xi} = \delta_{i,j}. \tag{6}$$

Here $W(\boldsymbol{\xi})$ is the weighting function corresponding to the Wiener-Askey polynomial chaos basis $\{H_i\}$. The gPC coefficients in Eqn. (5) are $a_i = \dfrac{\mathbb{E}[X(\omega)H_i(\boldsymbol{\xi}(\omega))]}{\mathbb{E}[H_i H_i]}$, $i = 0, \ldots, \infty$. These types of polynomial basis satisfy that the weighting function is the same as the probability function of $\boldsymbol{\xi}$. For Gaussian distribution, Gamma distribution, Beta distribution and Uniform distribution, such orthogonal polynomial sets are Hermite polynomials, Laguerre polynomials, Jacobi polynomials and Legendre polynomials respectively.

In this paper, we will focus on uniformly random variables. We use Legendre chaos in one dimension as an example. The one dimensional $(n+1)$th-order Legendre polynomials are defined as

$$H_{n+1}(\zeta) = \frac{\sqrt{2n+1}\sqrt{2n+3}}{n+1}\zeta H_n(\zeta) - \frac{n\sqrt{2n+3}}{(n+1)\sqrt{2n-1}} P_{n-1}(\zeta), -1 < \zeta < 1, \tag{7}$$

with

$$H_0(\zeta) = 1, \quad H_1(\zeta) = \sqrt{3}\zeta, \quad H_2 = \sqrt{5}(\frac{3}{2}\zeta^2 - \frac{1}{2}), \quad \ldots. \tag{8}$$

The weighting function in the orthogonality relation (6) is

$$W(\zeta) = \frac{1}{2}$$

Obviously, the weighting function is the same as the probability density function (PDF) of a uniform random variable $\zeta \sim U(-1, 1)$. Furthermore, by a tensor product representation, we can use the one-dimensional polynomial $H_i(\xi)$ to construct a sufficient orthonormal basis $\mathbf{H}_{\boldsymbol{\alpha}}(\boldsymbol{\xi})$'s of $L^2(\Omega)$ as follows

$$\mathbf{H}_{\boldsymbol{\alpha}}(\boldsymbol{\xi}) = \prod_{i=0}^{r} H_{\alpha_i}(\xi_i), \boldsymbol{\alpha} \in \Im_r^{\infty},$$

where $\boldsymbol{\alpha}$ is a multi-index and $\Im_r^{\infty}$ is a multi-index set of countable cardinality,

$$\Im_r^{\infty} = \{\boldsymbol{\alpha} = (\alpha_1, \alpha_2, \ldots, \alpha_r) | \alpha_i \geq 0, \alpha_i \in \mathcal{N}\}.$$

Here $\mathcal{N}$ is a set of non-negative integers. The zero multi-index corresponding to $\mathbf{H}_0(\boldsymbol{\xi}) = 1$, which is used to represent the mean of the solution. Clearly, the cardinality of $\Im_r^\infty$ is infinite. For the purpose of numerical computations, we prefer a finite set of polynomials. There are many choices of truncations. One possible choice is the set of polynomials whose total orders are at most p, *i.e.*,

$$\Im_r^p = \left\{ \boldsymbol{\alpha} | \boldsymbol{\alpha} = (\alpha_1, \alpha_2, \ldots, \alpha_r), \alpha_i \in \mathcal{N}, |\boldsymbol{\alpha}| = \sum_{i=1}^{r} \alpha_i \leq p \right\}. \tag{9}$$

The cardinality of $\Im_r^p$ in (9) or the number of polynomial basis functions, denoted by $N_p = |\Im_r^p|$, is equal to $(p+r)!/p!r!$. Another good choice is the sparse truncation method proposed in Luo's thesis [12]. We may simply write such a truncated set as $\Im$ when no ambiguity arises. The orthonormal basis $\mathbf{H}_{\boldsymbol{\alpha}}(\boldsymbol{\xi})$ is the standard generalized polynomial chaos (gPC) basis, see [25] for more details.

Next, we will introduce the solution procedure based on the generalized polynomial chaos framework. To simplify notations, we consider the following time-dependent stochastic differential equations:

$$\begin{aligned} \frac{dv}{dt} &= \mathcal{L}_v\{v, q, \omega\} = \frac{1}{\rho}\nabla \cdot \mathbf{k}\nabla v - I_{\text{ion}}(v, q), \\ \frac{dq}{dt} &= \mathcal{L}_q\{v, q, \omega\} = \alpha v - \beta q, \end{aligned} \tag{10}$$

with $x \in D$, $\omega \in \Omega$, $t \in [0, T]$. $\mathbf{k}(x, \omega)$ is the conductivity tensor defined on $D^{d\times d} \times \Omega$, with Ω defined as a proper probability space. Suitable initial and boundary conditions will be assumed later. By using the gPC expansion, we expand the random processes in the system of (10) follow the form below:

$$\begin{aligned} v(x, t; \omega) &= \sum_{i=0}^{M} v_i(x, t)\mathbf{H}_i(\boldsymbol{\xi}) \triangleq \mathbf{V}\hat{\mathbf{H}}^T, \\ q(x, t; \omega) &= \sum_{i=0}^{M} q_i(x, t)\mathbf{H}_i(\boldsymbol{\xi}) \triangleq \mathbf{Q}\hat{\mathbf{H}}^T, \end{aligned} \tag{11}$$

where row vectors $\mathbf{V} = (v_0, v_1, v_2, \ldots, v_M)$, $\mathbf{Q} = (q_0, q_1, q_2, \ldots, q_M)$, $\mathbf{K} = (k_0, k_1, k_2, \ldots, k_M)$ and $M = N_p - 1$. $\hat{\mathbf{H}}$ is the assemble vector of polynomial chaos $\{\mathbf{H}_i\}$ in an giving order and $\hat{\mathbf{H}}_0 = 1$. Note the multi-index can be ordered in an ascending order following a single index, for example, the graded lexicographic order. Similar expansions are applied to the initial conditions and boundary conditions. The random parameters also have the same formulation as other random processes:

$$\begin{aligned} k(x; \omega) &= \sum_{i=0}^{M} k_i(x)\mathbf{H}_i(\boldsymbol{\xi}) \triangleq \mathbf{K}\hat{\mathbf{H}}^T, \\ \lambda(\omega) &= \sum_{i=0}^{M} \lambda_i\mathbf{H}_i(\boldsymbol{\xi}) \triangleq \mathbf{L}\hat{\mathbf{H}}^T, \\ \theta(\omega) &= \sum_{i=0}^{M} \theta_i\mathbf{H}_i(\boldsymbol{\xi}) \triangleq \mathbf{T}\hat{\mathbf{H}}^T, \\ \alpha(\omega) &= \sum_{i=0}^{M} \alpha_i\mathbf{H}_i(\boldsymbol{\xi}) \triangleq \mathbf{A}\hat{\mathbf{H}}^T, \\ \beta(\omega) &= \sum_{i=0}^{M} \beta_i\mathbf{H}_i(\boldsymbol{\xi}) \triangleq \mathbf{B}\hat{\mathbf{H}}^T, \end{aligned} \tag{12}$$

where the row vectors are $\mathbf{K} = (k_0, k_1, k_2, \ldots, k_M)$, $\mathbf{L} = (\lambda_0, \lambda_1, \lambda_2, \ldots, \lambda_M)$, $\mathbf{T} = (\theta_0, \theta_1, \theta_2, \ldots, \theta_M)$, $\mathbf{A} = (\alpha_0, \alpha_1, \alpha_2, \ldots, \alpha_M)$, and $\mathbf{B} = (\beta_0, \beta_1, \beta_2, \ldots, \beta_M)$ respectively. The random parameter ω is absorbed into the polynomial basis, thus the expansion coefficients are deterministic. Next, a Galerkin projection is used to transform the stochastic governing equations into deterministic equations. Substitute the expansion into governing equation (10), we obtain

$$\begin{aligned} \frac{d\mathbf{V}}{dt}\hat{\mathbf{H}}^T &= \frac{1}{\rho}\nabla \cdot \mathbf{K}\hat{\mathbf{H}}^T \nabla \mathbf{V}\hat{\mathbf{H}}^T - I_{\text{ion}}(\mathbf{V}\hat{\mathbf{H}}^T, \mathbf{Q}\hat{\mathbf{H}}^T) \\ \frac{d\mathbf{Q}}{dt}\hat{\mathbf{H}}^T &= \mathbf{A}\hat{\mathbf{H}}^T\hat{\mathbf{H}}\mathbf{V}^T - \mathbf{B}\hat{\mathbf{H}}^T\hat{\mathbf{H}}\mathbf{Q}^T \end{aligned} \tag{13}$$

where

$$I_{\text{ion}}(\mathbf{V}\hat{\mathbf{H}}^T, \mathbf{Q}\hat{\mathbf{H}}^T) = -\mathbf{L}\hat{\mathbf{H}}^T(\mathbf{Q}\hat{\mathbf{H}}^T - \mathbf{T}\hat{\mathbf{H}}^T\hat{\mathbf{H}}\mathbf{V}^T - (1 + \mathbf{T}\hat{\mathbf{H}}^T)(\mathbf{V}\hat{\mathbf{H}}^T)^2 + (\mathbf{V}\hat{\mathbf{H}}^T)^3) \tag{14}$$

A Galerkin projection of the above equation onto each polynomial basis $\{\mathbf{H}_i\}$ is then conducted in order to ensure that the residual is orthogonal to the functional space spanned by the finite-dimensional basis $\{\mathbf{H}_i\}$. By projecting with $\mathbf{H}_i$ for each $i = \{0, \ldots, M\}$ and applying the orthogonality relation (6), we obtain the following system:

$$\begin{aligned} \frac{d\mathbf{V}}{dt} &= \mathbb{E}[\frac{1}{\rho}\nabla \cdot \mathbf{K}\hat{\mathbf{H}}^T \nabla \mathbf{V}\hat{\mathbf{H}}^T\hat{\mathbf{H}}] - \mathbb{E}[I_{\text{ion}}(\mathbf{V}\hat{\mathbf{H}}^T, \mathbf{Q}\hat{\mathbf{H}}^T)\hat{\mathbf{H}}] \\ \frac{d\mathbf{Q}}{dt} &= \mathbb{E}[\mathbf{A}\hat{\mathbf{H}}^T\hat{\mathbf{H}}\mathbf{V}^T\hat{\mathbf{H}}] - \mathbb{E}[\mathbf{B}\hat{\mathbf{H}}^T\hat{\mathbf{H}}\mathbf{Q}^T\hat{\mathbf{H}}] \end{aligned} \tag{15}$$

where

$$\begin{aligned} \mathbb{E}[I_{\text{ion}}(v,q)\hat{\mathbf{H}}] = \mathbb{E}[\mathbf{L}\hat{\mathbf{H}}^T\hat{\mathbf{H}}\mathbf{Q}^T\hat{\mathbf{H}}] - \mathbb{E}[\mathbf{L}\hat{\mathbf{H}}^T\hat{\mathbf{H}}\mathbf{V}^T\mathbf{V}\hat{\mathbf{H}}^T\hat{\mathbf{H}}] + \mathbb{E}[\mathbf{L}\hat{\mathbf{H}}^\mathbf{T}\hat{\mathbf{H}}\mathbf{V}^\mathbf{T}\mathbf{V}\hat{\mathbf{H}}^\mathbf{T}\hat{\mathbf{H}}\mathbf{V}^\mathbf{T}\hat{\mathbf{H}}] \\ + \mathbb{E}[\mathbf{L}\hat{\mathbf{H}}^T\hat{\mathbf{H}}\mathbf{V}^T\mathbf{T}\hat{\mathbf{H}}^T\hat{\mathbf{H}}] - \mathbb{E}[\mathbf{L}\hat{\mathbf{H}}^T\hat{\mathbf{H}}\mathbf{V}^T\mathbf{T}\hat{\mathbf{H}}^T\hat{\mathbf{H}}\mathbf{V}^T\hat{\mathbf{H}}] \end{aligned} \tag{16}$$

The above equation (15) is a set of N_p coupled partial differential equations. The initial conditions and boundary conditions are expanded in the same form as (11). By matching the coefficients in the expansions, we obtain the initial conditions and boundary conditions for each expanded equation in Eqn. (15) to complete the system. By solving the system (15), we have an approximate solution to the Spde (10) as follows

$$v_{\text{gPC}} = \sum_{i=0}^{M} v_i(x,t)H_i(\xi).$$

The gPC procedure of the HH mono-domain models is the same while we can not precisely compute the multiple tensor product $\mathbb{E}[I_{\text{ion}}(v,q)\hat{\mathbf{H}}]$. For the nonlinear functions in the HH model, there are exponential type functions in both denominator and numerator, we use Gauss points to compute the integration approximately.

The fourth order Runge-Kutta (RK4) methods are used for time discretization which can decouple the system (15) and center difference is used for space discretization .

Finally, Smolyak's method [18] is utilized to generate the collocation nodes and the collocation weights. Set the collocation nodes are $\{\xi_j\}_{j=1}^{N_s}$ which create N_s sets parameters $\{z_j\}_{j=1}^{N_s}$, and the collocation weights are $\{w_j\}_{j=1}^{N_s}$. Let $v_j(x,t)$ be the solution of governing equation Eq. (1) with a fixed value z_j. Then the mean solution is followed as

$$\bar{v}_{\mathrm{SC}} = \sum_{j=1}^{N_s} w_j v_j(x,t),$$

and the variance of the solution is

$$D(v_{\mathrm{SC}}) = \sum_{j=1}^{N_s} w_j (v_j(x,t) - \bar{v}_{SC})^2.$$

It is also possible to calculate the mean and the variance of the solution's derivative as

$$\frac{d\bar{v}_{\mathrm{SC}}}{dt} = \sum_{j=1}^{N_s} w_j \frac{dv_j(x,t)}{dt},$$

and

$$D(\frac{dv_{\mathrm{SC}}}{dt}) = \sum_{j=1}^{N_s} w_j (\frac{dv_j(x,t)}{dt} - \frac{d\bar{v}_{\mathrm{SC}}}{dt})^2.$$

4 NUMERICAL RESULTS

4.1 Fitz-Hugh Nagumo Model

We consider the dimensionless FHN monodomain model in two space dimensions

$$\begin{cases} \dfrac{\partial v}{\partial t} &= \dfrac{1}{\rho}\nabla\cdot(k\nabla v) + \lambda(q - v(1-v)(v-\theta)) \\ \dfrac{\partial q}{\partial t} &= \alpha v - \beta q \end{cases} \tag{17}$$

for $t > 0$ and $x = (x_1, x_2)^T \in (0,1)^2$, with deterministic parameters: $\dfrac{1}{\rho} = 0.01$, $\lambda = -100$, $\theta = 0.25$, $\alpha = 0.16875$, $\beta = 1.0$ and $k = 1$. We give an initial stimulus at the lower left corner of this square as followed:

$$\begin{aligned} v(x,0) &= \frac{1}{1 + e^{50(\sqrt{x_1^2 + x_2^2} - 0.1)}} \\ q(x,0) &= 0, \end{aligned} \tag{18}$$

and homogeneous Neumann boundary conditions are applied. In the experiments, the space step size is $\Delta x = 1/128$ and the time step size is $\Delta t = 0.001$. In the following part, we analyze the effects of uncertainty on the deterministic solution by giving the model parameters different types of perturbation.

4.1.1 Deterministic perturbation

Firstly, we observe four metrics of action potential shape (action potential duration (APD), action potential duration to 90% polarization (APD90), the derivative of voltage, max v), one metrics of action potential propagation (conduction time) and the solution itself at a fixed time and a given point with different parameters. Here, the conduction time is calculated by the first recording the time taken for an upstroke to begin at the furthest location from the stimulus.

For simplicity, let the perturbation be deterministic. The model parameters vary with a change

of $\pm 15\%$ around the default values, *i.e.*, $|c_z| \leq 0.15$. This range can assure that there is an upstroke with different perturbation. We can scale this total range normalized to range from -1 to 1, *i.e.*, 0 represents the original values. In this setting, we can quantitatively analyze the influences of model parameters (ϵ, λ, α, β, θ and $v(x,0)$) to the outputs were given. The outputs change with the model parameters change around their default values and the results are shown in Fig. 1.

The Fig. 1(a) shows that the solution is continuous on all the model parameters and differentiable to all the model parameters. That allows us to give the solution a Taylor expansion analysis when the perturbation is small enough. According to Fig. 1, we can observe that the model parameter θ has strong effects on all the outputs. The parameters α and β have a strong effect on APD and APD90 which means the action potential shape is most sensitive to a and β. Furthermore, the ionic dynamics $\mathcal{M}$ have a strong effect on the shape of the AP. The voltage derivative is restricted at some fixed point and fixed time, and sensitive to all the parameters. The parameters θ, λ and α have a significant influence on the maximum voltage. And numerical results show that the maximum voltage does not change a lot once there exists an upstroke. The conduction times is much sensitive to θ which means the conduction velocity is not only influenced by the diffusion parameter k.

Above all, we can demonstrate that the parameters λ and θ which are contained in the dynamics I_{ion} have large effects on all the outputs. APD and APD90 have the same behavior, and they are most sensitive to the parameters α and β. It is easy to see that the computation accuracy of APD, APD90 and time for conduction is limited by the time step size Δt.

4.1.2 Random perturbation

Next, we focus on the effects of small random perturbation to the original solution. Assume that the expectation of the random perturbation is 0 and only one model parameter is perturbed at a time. Since the perturbation is uniformly distributed, we can rewrite the perturbation coefficient c_z as $c\xi$, $\xi \sim U(-1,1)$. In this assumption, the standard variance of the randomized parameter is $\sigma(c\xi) = \frac{1}{3}|c|$. When the random perturbation is sufficiently small, we can get a quadratic relationship between the std of the randomized parameter and the expectation of the difference between the original solution and the stochastic solution. Meanwhile, there is a positive linear relationship between the std of randomized parameter and the std of the difference.

Let $Y_z(c_z)$ be the outputs that we observe with one parameter z is randomly perturbed c_z. Since the limitation to the computation accuracy, we give the results of Y represents solution itself and derivation of voltage. In stochastic case, the difference $\Delta Y_z(c_z) = Y_z(c_z) - Y_z(c_z = 0)$ is a random variable. Generally, the first and the second moment are the most commonly used information to analyze the stochastic variables. So we try to analysis the relationship between difference's finite moment and the finite moment of the random perturbation. The numerical results show that the expectation of the difference is quadratically proportional to the std of the perturbation c_z and the standard variance (std) of the difference is linearly proportional to the std of the perturbation c_z. The relationship can be represented in the following formula:

$$
\begin{aligned}
E[\Delta Y_z(c_z)] &= \frac{\partial^2 Y_z}{\partial c_z^2}\sigma(c_z)^2, \\
\sigma(\Delta Y_z(c_z)) &= |\frac{\partial Y_z}{\partial c_z}|\sigma(c_z),
\end{aligned}
\tag{19}
$$

Figs. 2 and 3 illustrate the results of $Y = v(x,t)$. The results for derivation of voltage is shown in Figs. 4 and 5. And the slope of the lines in Figs. 3 and 5 is positive which is consistent with that the coefficient in (19) is positive.

We also can get the conclusion that the standard variance varies markedly along the space. Its value is large where the mean solution changes fast with a fixed random perturbation. There is a known property that an action potential consists of five phases: upstroke or depolarization, early re-polarization, plateau, re-polarization and resting. A second action potential cannot be triggered immediately after an action potential upstroke which causes the phenomenon called refractoriness. The time during which it is not possible to trigger a second action potential is familiar as the refractory period. Here, a second stimulus given by

$$
I_{stim} = \begin{cases} 1 & \text{if} \sqrt{(x_1 - 0.5)^2 + (x_2 - 0.5)^2} < 0.2 \\ 0 & \text{otherwise} \end{cases}
$$

is applied to the membrane potential around the center of the domain at time $t = 4$. We observe the mean and the standard variance of the stochastic solution giving k a random perturbation. Set $c_k = 0.05\xi$, $\xi \sim U(-1, 1)$. Fig. 6 displays the results at some fixed time.

According to the results, there still exists a spiral wave phenomenon when the random perturbation is small. Fig. 6(a) shows only half of the second action potential can be propagated. Fig. 6 shows that the standard variance is almost zeros except for space where mean solution changes fast.

4.2 Hodgkin-Huxley Model

In this subsection, we consider the HH monodomain model in two space dimensions

$$
\begin{cases}
\dfrac{\partial v}{\partial t} &= \dfrac{1}{\rho}\nabla\cdot(k\nabla v) - (\bar{g}_{\mathrm{Na}} m^3 h(v - E_{\mathrm{Na}}) + \bar{g}_{\mathrm{K}} n^4 (v - E_{\mathrm{K}}) + g_{\mathrm{leak}}(v - E_{\mathrm{leak}})) \\
\dfrac{\partial m}{\partial t} &= (1 - m)\alpha_m(v) - m\beta_m(v) \\
\frac{\partial h}{\partial t} &= (1 - h)\alpha_h(v) - h\beta_h(v) \\
\dfrac{\partial n}{\partial t} &= (1 - n)\alpha_n(v) - n\beta_n(v)
\end{cases}
\tag{20}
$$

for $t > 0$ and $x = (x_1, x_2)^T \in (0,1)^2$, with deterministic parameters: $\frac{1}{\rho} = 0.01$, $\bar{g}_{\mathrm{Na}} = 120$, $E_{\mathrm{Na}} = 115$, $\bar{g}_{\mathrm{K}} = 36$, $E_{\mathrm{K}} = -12$, $\bar{g}_{\mathrm{leak}} = 0.3$, $E_{\mathrm{leak}} = 10.613$, $k = 1$. Here, the rate functions are given by

$$\begin{aligned}
\alpha_m(v) &= 0.1\frac{25-v}{\exp(\frac{25-v}{10})-1}, \quad \beta_m(v) = 4.0\exp(-\frac{v}{18}); \\
\alpha_h(v) &= 0.07\exp(\frac{-v}{20}), \quad \beta_h(v) = \frac{1}{\exp(\frac{30-v}{10})+1}; \\
\alpha_n(v) &= 0.01\frac{10-v}{\exp(\frac{10-v}{10})-1}, \quad \beta_n(v) = 0.125\exp(-\frac{v}{80});
\end{aligned}$$

Set the initial stimulus at the lower left corner of this square is as followed:

$$\begin{aligned}
v(x,0) &= 0.003621 + \frac{20}{1+e^{20(\sqrt{x_1^2+x_2^2}-0.5)}} \\
m(x,0) &= 0.052955 \\
h(x,0) &= 0.595994 \\
n(x,0) &= 0.317732
\end{aligned} \tag{21}$$

and homogeneous Neumann boundary conditions are applied. The space step size and the time step size is the same as the space step size and the time step size in section 4.1. Then, we analyze the effects of uncertainty on the deterministic solution by giving the model parameters different types of perturbation.

We only consider the case that one of the parameters k, $\bar{g}_{\mathrm{Na}}$, E_{Na}, v, has a random perturbation. Other parameters have the same default values.

Same as before, we first consider the perturbation is deterministic and quantitatively analyze the influences of model parameters on the six metrics (v, APD, APD90, max v, $\frac{dv}{dt}$, conduction times). Set the model parameters vary with a change of $\pm 15\%$ around the default values. Fig. 7(a) shows the continuity and differentiability of the model parameters. The parameter E_{Na} represents the value of the sodium reversal potential. Fig. 7 illustrates that the parameter E_{Na} has a strong influence on APD and APD90, also has an impact on other outputs. Except for the parameter E_{Na}, other parameters rarely affect the maximum voltage.

When the perturbation is a random variable and small enough, we also get the quadratic relationship and the linear relationship which described as the Eqn. (19). Fig. 8 displays that the expectation of the difference $\Delta Y_z = v(x,t;c_z) - v(x,t)$ is quadratically proportional to the standard variance of the perturbation c_z while Fig. 9 shows the standard variance of the difference is linearly proportional to $\sigma(c_z)$. Figs. 10 and 11 illustrate the same conclusion when the output is the derivation of the voltage.

An simple explanation of the results (19) is given. Numerical results show that the outputs $Y_z(c_z)$ are continuous and differentiable to the model parameters. So when the perturbation is small enough, we can take Taylor expansion to the $Y_z(c_z)$ as follows

$$Y_z(c_z) = Y_z(c_z = 0) + \frac{\partial Y_z}{\partial c_z} c_z + \frac{1}{2} \frac{\partial^2 Y_z}{\partial c_z^2} c_z^2 + o(c_z^2). \tag{22}$$

The difference is as followed

$$\begin{aligned} \Delta Y_z &= Y_z(c_z) - Y_z(c_z = 0) \\ &= \frac{\partial Y_z}{\partial c_z} c_z + \frac{1}{2} \frac{\partial^2 Y_z}{\partial c_z^2} c_z^2 + o(c_z^2). \end{aligned} \tag{23}$$

Note ΔY_z is the difference between the original output Y and the perturbed solution $Y_z(c_z)$. It is obvious that the difference ΔY_z is linearly proportional to the perturbation c_z when it is small enough.

In stochastic case, the difference ΔY_z is a random variable. We already have the Taylor expansion of the perturbed outputs Y_z and formulation (23) of ΔY_z. Firstly, both sides of the Eqn. (23) take expectation

$$\begin{aligned} \mathbb{E}(\Delta Y_z) &= \mathbb{E}(\frac{\partial Y_z}{\partial c_z} c_z + \frac{1}{2} \frac{\partial^2 Y_z}{\partial c_z^2} c_z^2 + o(c_z^2)) \\ &= \frac{1}{2} \frac{\partial^2 Y_z}{\partial c_z^2} \mathbb{E}(c_z^2) + o(\mathbb{E}(c_z^2)) \\ &\approx \frac{1}{2} \frac{\partial^2 Y_z}{\partial c_z^2} \sigma(c_Z)^2 \end{aligned} \tag{24}$$

Next, both sides of the Eqn. (23) take variance

$$\begin{aligned} D(\Delta Y_z) &= D(\frac{\partial Y_z}{\partial c_z} c_z + \frac{\partial^2 Y_z}{\partial c_z^2} \cdot \frac{1}{2} c_z^2 + o(c_z^2)) \\ &= (\frac{\partial Y_z}{\partial c_z})^2 \sigma(c_z)^2 + o(c_z^2) \\ &\approx (\frac{\partial Y_z}{\partial c_z})^2 \sigma(c_z)^2 \end{aligned} \tag{25}$$

So the std of the difference satisfies

$$\sigma(\Delta Y_Z) \approx |\frac{\partial Y_z}{\partial c_z}| \sigma(c_Z)$$

We notice that the coefficient $|\frac{\partial Y_z}{\partial c_z}| > 0$. So we can get the results that the expectation of the difference is quadratically proportional to the std of the perturbation c_z and the standard variance (std) of the difference is linearly proportional to the std of the perturbation c_z. The relationships

are shown as follows

$$\begin{aligned} E[\Delta Y_z(c_z)] &= \frac{\partial^2 Y_z}{\partial c_z^2}\sigma(c_z)^2, \\ \sigma(\Delta Y_z(c_z)) &= |\frac{\partial Y_z}{\partial c_z}|\sigma(c_z). \end{aligned} \tag{26}$$

The quadratically fitting coefficient $\frac{\partial^2 Y_z}{\partial c_z^2}$ should be the same as the second order derivative at 0 when the perturbation is deterministic. Meanwhile, the linearly fitting coefficient $|\frac{\partial Y_z}{\partial c_z}|$ should be the same as the first order derivative at 0 when perturbation is deterministic. Numerical results show that the coefficients $\frac{\partial^2 Y_z}{\partial c_z^2}$ and $|\frac{\partial Y_z}{\partial c_z}|$ getting from gPC method and SC method are almost the same as the derivatives at 0.

5 CONCLUSIONS

In order to improve the model reliability, this paper presents an explorative research on the effects of the uncertainties by observing the difference arising from parameters uncertainties. Firstly, each parameter has different effects on the solution responses. Then, the numerical results show that the expectation of the solution converges to the original solution at a speed of order 2. Meanwhile, the std of the solution converges linearly proportional to the std of the perturbation. And the standard variance of the solution has spatial variability., *i.e.*, the standard variance is large where the mean solution changes fast. With these conclusions in mind, we should stress that the numerical results are not confined to the mono-domain equations with FHN model or HH model as long as the outputs surface are smooth to the parameters. Finally, there are some properties we can consider further, including spiral wave phenomenon and its chaotic behavior with longtime simulation.

Acknowledgements

The research of W. Ying is partially supported by NSFC grant DMS-11771290. The research of Z. Zhang is supported by Hong Kong RGC grants (Projects 27300616 and 17300318), National Natural Science Foundation of China (Project 11601457), Seed Funding Programme for Basic Research (HKU), and the Hung Hing Ying Physical Sciences Research Fund (HKU).

References

[1] I. Babuska, F. Nobile, and R. Tempone. A stochastic collocation method for elliptic partial differential equations with random input data. *SIAM J. Numer. Anal.*, 45:1005–1034, 2007.

[2] Eugene TY Chang and Richard H Clayton. Uncertainty and sensitivity analysis of the courtemanche-ramirez-nattel human atrial cell model using gaussian process emulators. In *Computing in Cardiology Conference (CinC), 2015*, pages 857–860. IEEE, 2015.

[3] Eugene TY Chang, Mark Strong, and Richard H Clayton. Bayesian sensitivity analysis of a cardiac cell model using a gaussian process emulator. *PLoS One*, 10(6):e0130252, 2015.

[4] Mulin Cheng, Thomas Y Hou, and Zhiwen Zhang. A dynamically bi-orthogonal method for time-dependent stochastic partial differential equations i: Derivation and algorithms. *Journal of Computational Physics*, 242:843–868, 2013.

[5] Mulin Cheng, Thomas Y Hou, and Zhiwen Zhang. A dynamically bi-orthogonal method for time-dependent stochastic partial differential equations ii: Adaptivity and generalizations. *Journal of Computational Physics*, 242:753–776, 2013.

[6] RH Clayton, Olivier Bernus, EM Cherry, Hans Dierckx, Flavio H Fenton, L Mirabella, Alexander V Panfilov, Frank B Sachse, Gunnar Seemann, and H Zhang. Models of cardiac tissue electrophysiology: progress, challenges and open questions. *Progress in biophysics and molecular biology*, 104(1-3):22–48, 2011.

[7] Piero Colli Franzone, Peter Deuflhard, Bodo Erdmann, Jens Lang, and Luca F Pavarino. Adaptivity in space and time for reaction-diffusion systems in electrocardiology. *SIAM Journal on Scientific Computing*, 28(3):942–962, 2006.

[8] R. Ghanem and P. Spanos. *Stochastic finite elements: a spectral approach.* Springer-Verlag, New York, 1991.

[9] Alan L Hodgkin and Andrew F Huxley. A quantitative description of membrane current and its application to conduction and excitation in nerve. *The Journal of physiology*, 117(4):500–544, 1952.

[10] Ross H Johnstone, Eugene TY Chang, Rémi Bardenet, Teun P De Boer, David J Gavaghan, Pras Pathmanathan, Richard H Clayton, and Gary R Mirams. Uncertainty and variability in models of the cardiac action potential: Can we build trustworthy models? *Journal of molecular and cellular cardiology*, 96:49–62, 2016.

[11] Svein Linge, Joakim Sundnes, Monica Hanslien, Glenn Terje Lines, and Aslak Tveito. Numerical solution of the bidomain equations. *Philosophical Transactions of the Royal Society of London A: Mathematical, Physical and Engineering Sciences*, 367(1895):1931–1950, 2009.

[12] Wuan Luo. *Wiener chaos expansion and numerical solutions of stochastic partial differential equations.* PhD thesis, California Institute of Technology, 2006.

[13] X. Ma and N. Zabaras. An adaptive hierarchical sparse grid collocation algorithm for the solution of stochastic differential equations. *J. Comput. Phys.*, 228:3084–3113, 2009.

[14] Gary R Mirams, Pras Pathmanathan, Richard A Gray, Peter Challenor, and Richard H Clayton. Uncertainty and variability in computational and mathematical models of cardiac physiology. *The Journal of physiology*, 594(23):6833–6847, 2016.

[15] Eleonora Musharbash, Fabio Nobile, and Tao Zhou. Error analysis of the dynamically orthogonal approximation of time dependent random pdes. *SIAM Journal on Scientific Computing*, 37(2):A776–A810, 2015.

[16] Habib N Najm. Uncertainty quantification and polynomial chaos techniques in computational fluid dynamics. *Annual review of fluid mechanics*, 41:35–52, 2009.

[17] T. Sapsis and P. Lermusiaux. Dynamically orthogonal field equations for continuous stochastic dynamical systems. *Physica D: Nonlinear Phenomena*, 238:2347–2360, 2009.

[18] Sergey Smolyak. Quadrature and interpolation formulas for tensor products of certain classes of functions. In *Soviet Math. Dokl.*, volume 4, pages 240–243, 1963.

[19] Tao Tang and Tao Zhou. Recent developments in high order numerical methods for uncertainty quantification. *Scientia Sinica Mathematica*, 45(7):891–928, 2015.

[20] John A. Trangenstein, Kirill Skouibine, and William K. Allard. Operator splitting and adaptive mesh refinement for the fitzhugh-nagumo problem. 2000.

[21] EJ Vigmond, R Weber Dos Santos, AJ Prassl, M Deo, and G Plank. Solvers for the cardiac bidomain equations. *Progress in biophysics and molecular biology*, 96(1-3):3–18, 2008.

[22] Norbert Wiener. The homogeneous chaos. *American Journal of Mathematics*, 60(4):897–936, 1938.

[23] D. Xiu. Fast numerical methods for stochastic computations: a review. *Commun. Comput. Phys.*, 5:242–272, 2009.

[24] D. Xiu and G. Karniadakis. Modeling uncertainty in flow simulations via generalized polynomial chaos. *J. Comput. Phys.*, 187:137–167, 2003.

[25] Dongbin Xiu and George Em Karniadakis. The wiener–askey polynomial chaos for stochastic differential equations. *SIAM journal on scientific computing*, 24(2):619–644, 2002.

[26] Wenjun Ying. *A multilevel adaptive approach for computational cardiology.* Duke University, 2005.

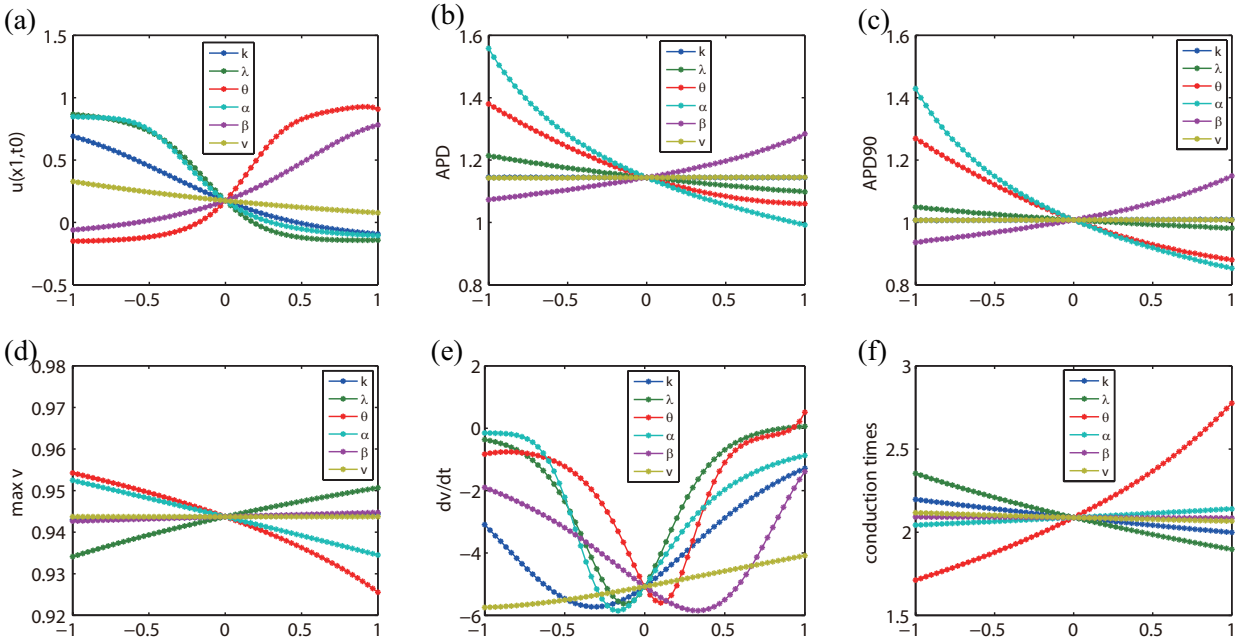

Figure 1: (a): the effects of model parameters on $v(x,t;c_z)$ at time $t=3.0$ and point $x=(0.5,0.5)$; (b): the effects of model parameters on APD; (c): the effects of model parameters on APD90; (d): the effects of model parameters on $\frac{dv}{dt}$; (e): the effects of model parameters on maximum voltage; (f): the effects of model parameters on conduction times from the lower left corner to the upper right corner.

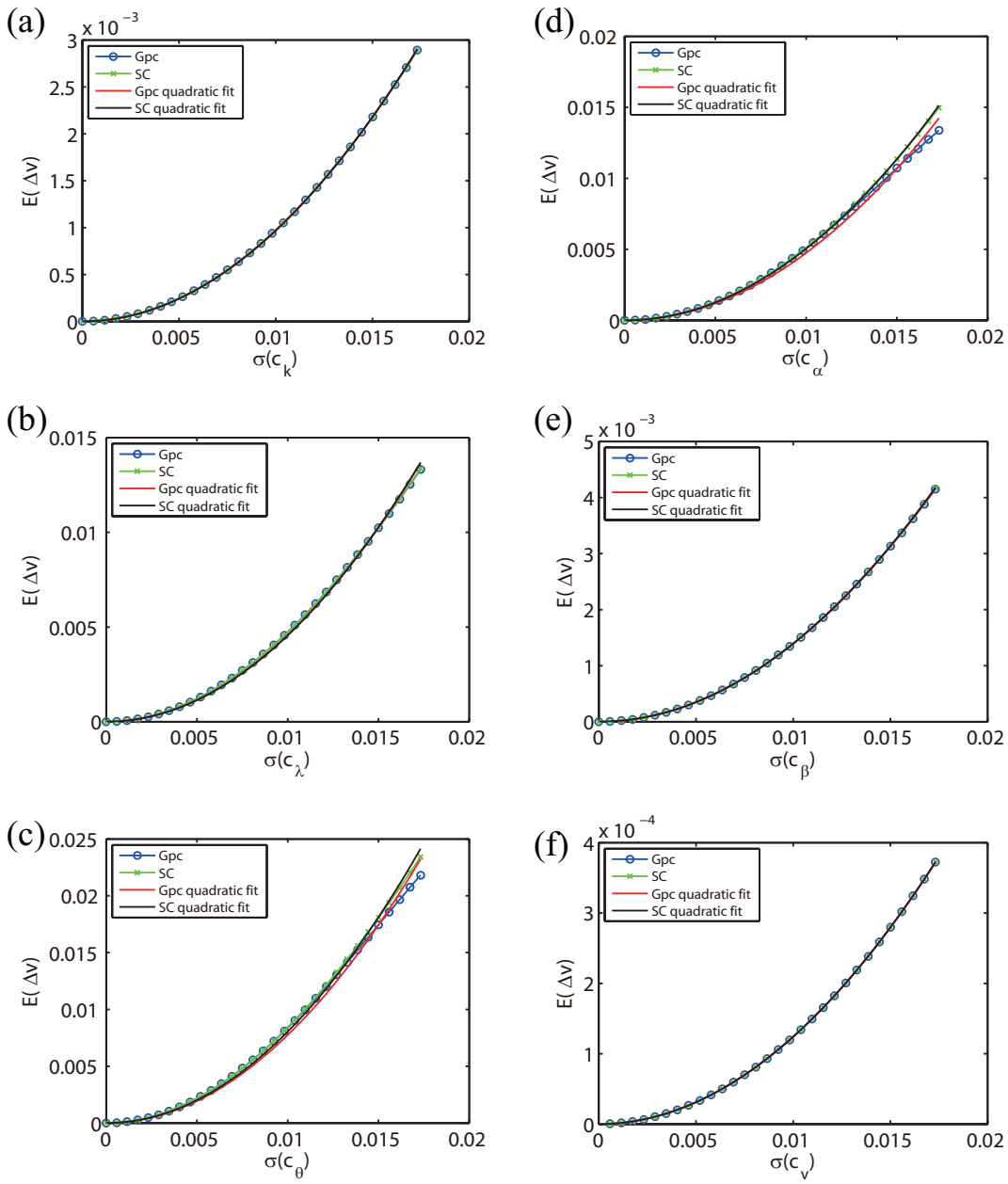

Figure 2: We observe the solution itself, *i.e.*, $\Delta Y_z = v(x,t;c_z) - v(x,t)$. Fix at a point $x = (0.5, 0.5)$ and in time $T = 3.0$. The blue lines are the numerical results of gPC and the red lines are the quadratically fitting lines; the green lines are the numerical results of SC and the black lines are the quadratically fitting lines. (a): only k has a random perturbation; (b): only λ has a random perturbation; (c): only θ has a random perturbation; (d): only α has a random perturbation; (e): only β has a random perturbation; (f): only $v(x,0)$ has a random perturbation; The quadratic relationship is shown.

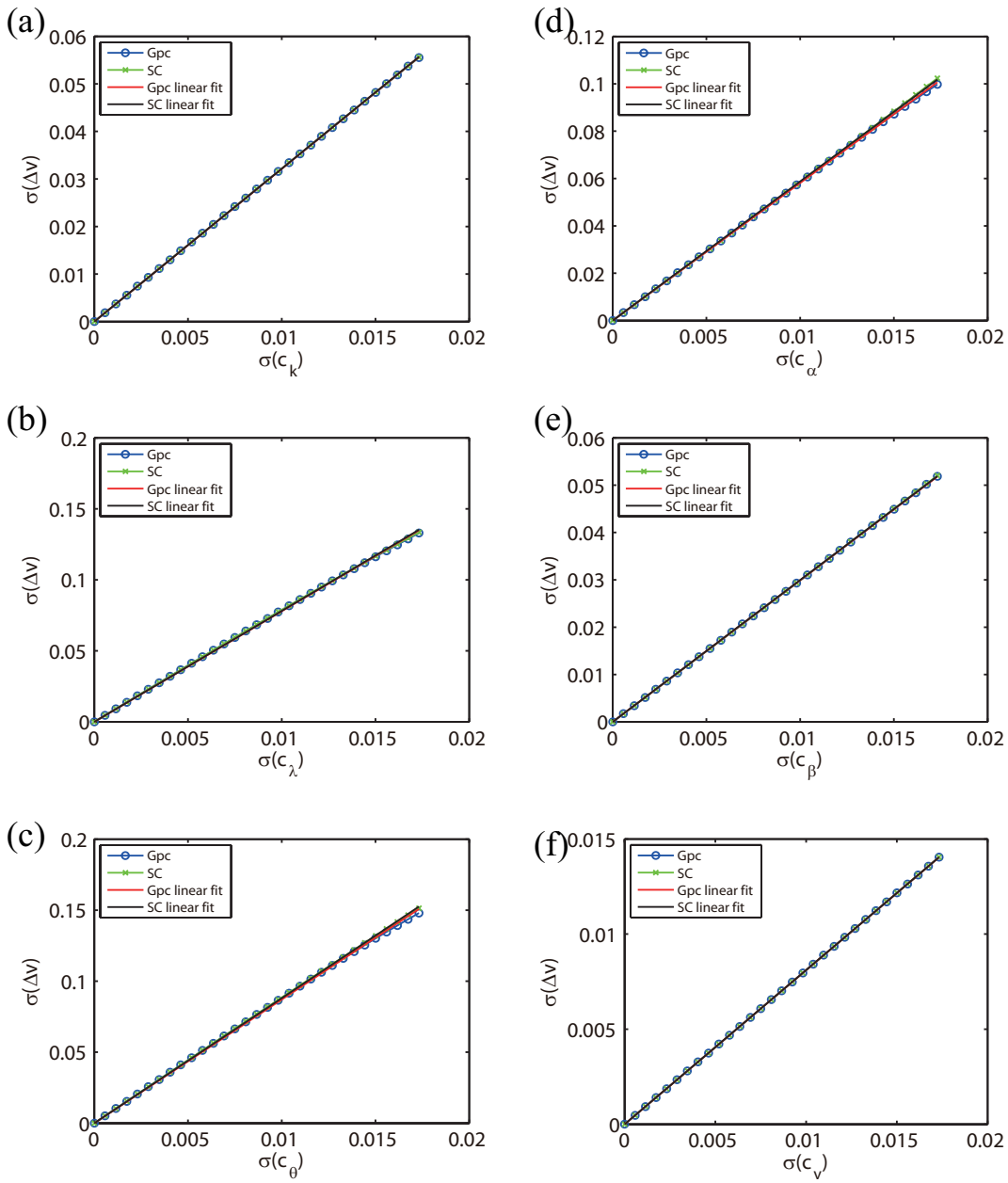

Figure 3: We observe the solution itself, *i.e.*, $\Delta Y_z = v(x,t;c_z) - v(x,t)$. Fix at a point $x = (0.5, 0.5)$ and in time $T = 3.0$. The blue lines are the numerical results of gPC and the red lines are the linearly fitting lines; the green lines are the numerical results of SC and the black lines are the linearly fitting lines. (a): only k has a random perturbation; (b): only λ has a random perturbation; (c): only θ has a random perturbation; (d): only α has a random perturbation; (e): only β has a random perturbation; (f): only $v(x,0)$ has a random perturbation; The linear relationship is shown.

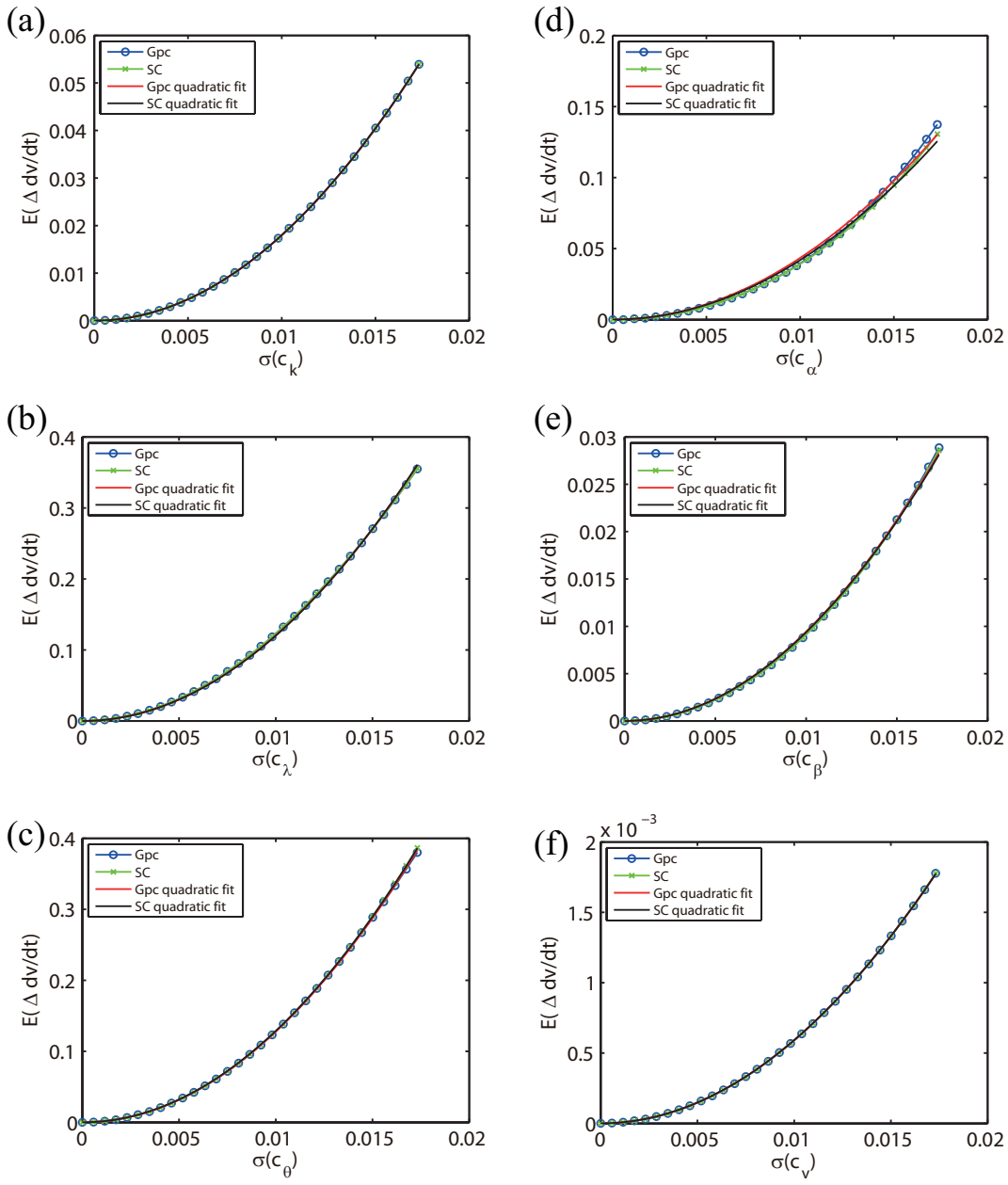

Figure 4: We observe the voltage derivative, *i.e.*, $\Delta Y_z = \dfrac{dv(x,t;c_z)}{dt} - \dfrac{dv(x,t)}{dt}$. Fix at a point $x = (0.5, 0.5)$ and in time $T = 3.0$. The blue lines are the numerical results of gPC and the red lines are the quadratically fitting lines; the green lines are the numerical results of SC and the black lines are the quadratically fitting lines. (a): only k has a random perturbation; (b): only λ has a random perturbation; (c): only θ has a random perturbation; (d): only α has a random perturbation; (e): only β has a random perturbation; (f): only $v(x,0)$ has a random perturbation; The quadratic relationship is shown.

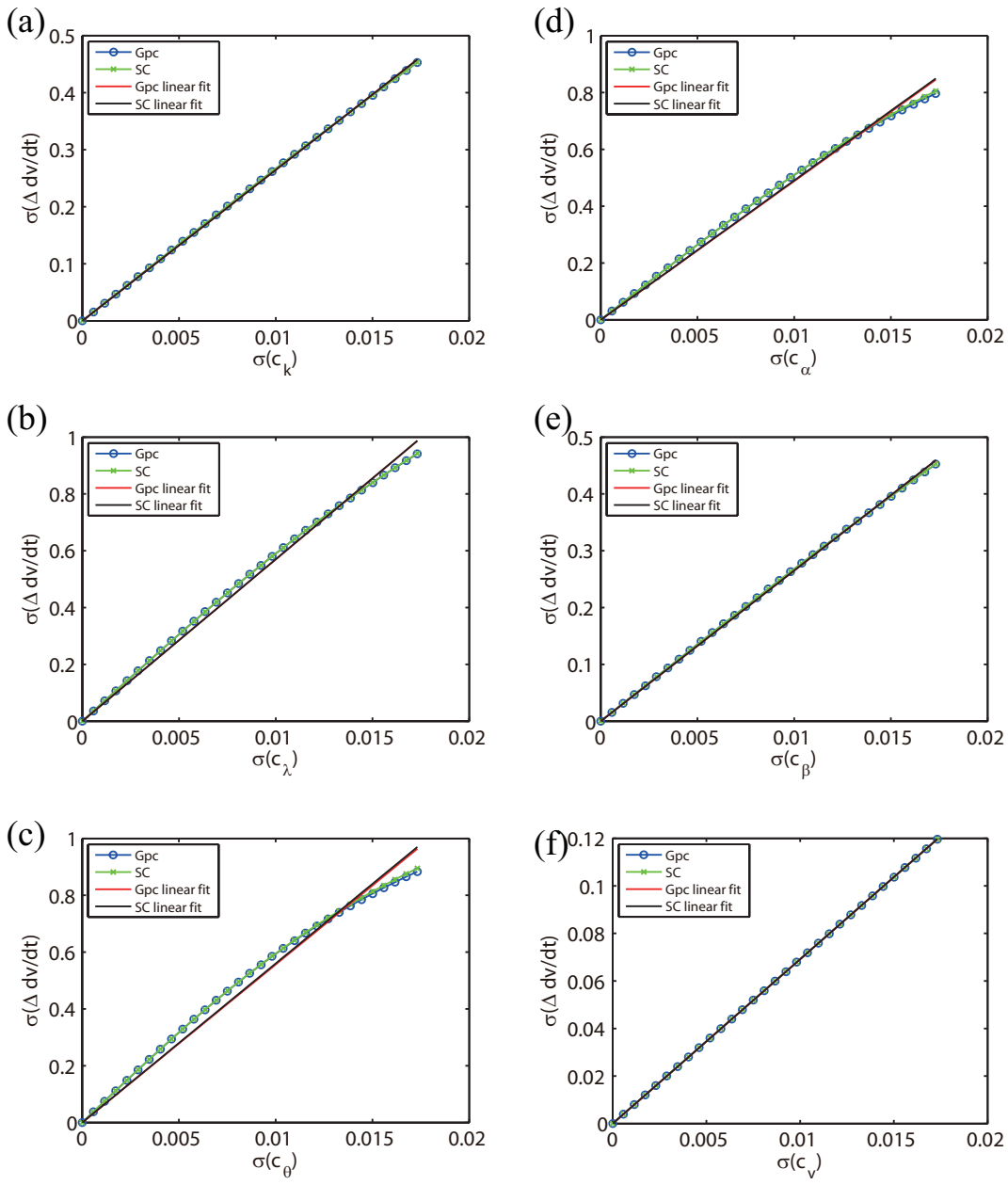

Figure 5: We observe the voltage derivative, *i.e.*, $\Delta Y_z = \dfrac{dv(x,t;c_z)}{dt} - \dfrac{dv(x,t)}{dt}$. Fix at a point $x = (0.5, 0.5)$ and in time $T = 3.0$. The blue lines are the numerical results of gPC and the red lines are the linearly fitting lines; the green lines are the numerical results of SC and the black lines are the linearly fitting lines. (a): only k has a random perturbation; (b): only λ has a random perturbation; (c): only θ has a random perturbation; (d): only α has a random perturbation; (e): only β has a random perturbation; (f): only $v(x,0)$ has a random perturbation; The linear relationship is shown.

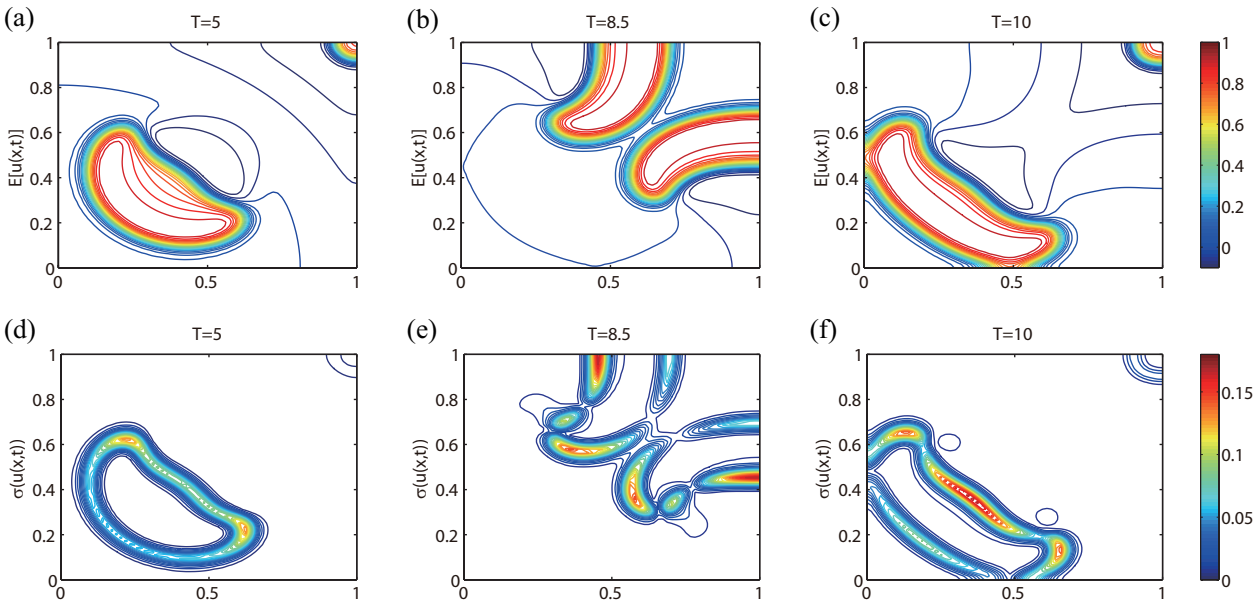

Figure 6: The sub-figures on the top line display the mean solutions while the sub-figures on the bottom line display the standard variances of the solutions. (a): at time $t = 5$, only half of the second action potential can be propagated; (b): at time $t = 8.5$, the half stimulation generates the new wave; (c): at time $t = 10$, the wave fused in the shape of semicircle approximately; (d): the standard variance at time $t = 5$; (d): the standard variance at time $t = 8.5$; (d): the standard variance at time $t = 10$;

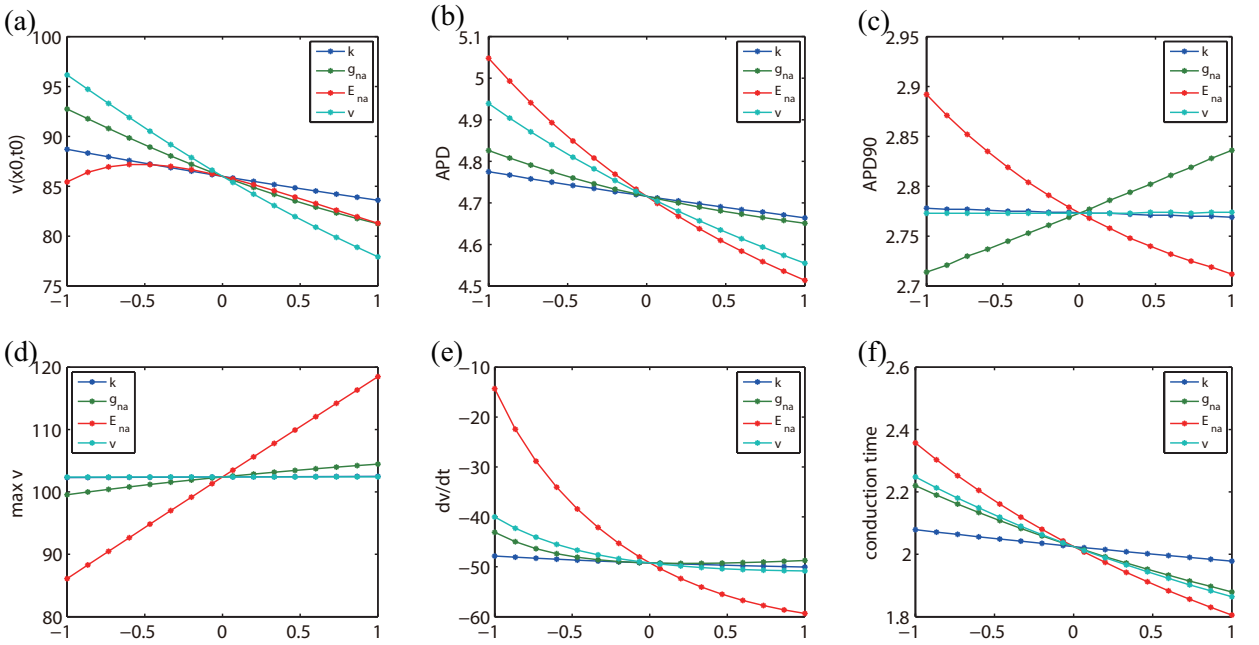

Figure 7: (a): the effects of model parameters on $v(x, t; c_z)$ at time $t = 3.0$ and point $x = (0.5, 0.5)$; (b): the effects of model parameters on APD; (c): the effects of model parameters on APD90; (d): the effects of model parameters on $\dfrac{dv}{dt}$; (e): the effects of model parameters on maximum voltage; (f): the effects of model parameters on conduction times from the lower left corner to the upper right corner.

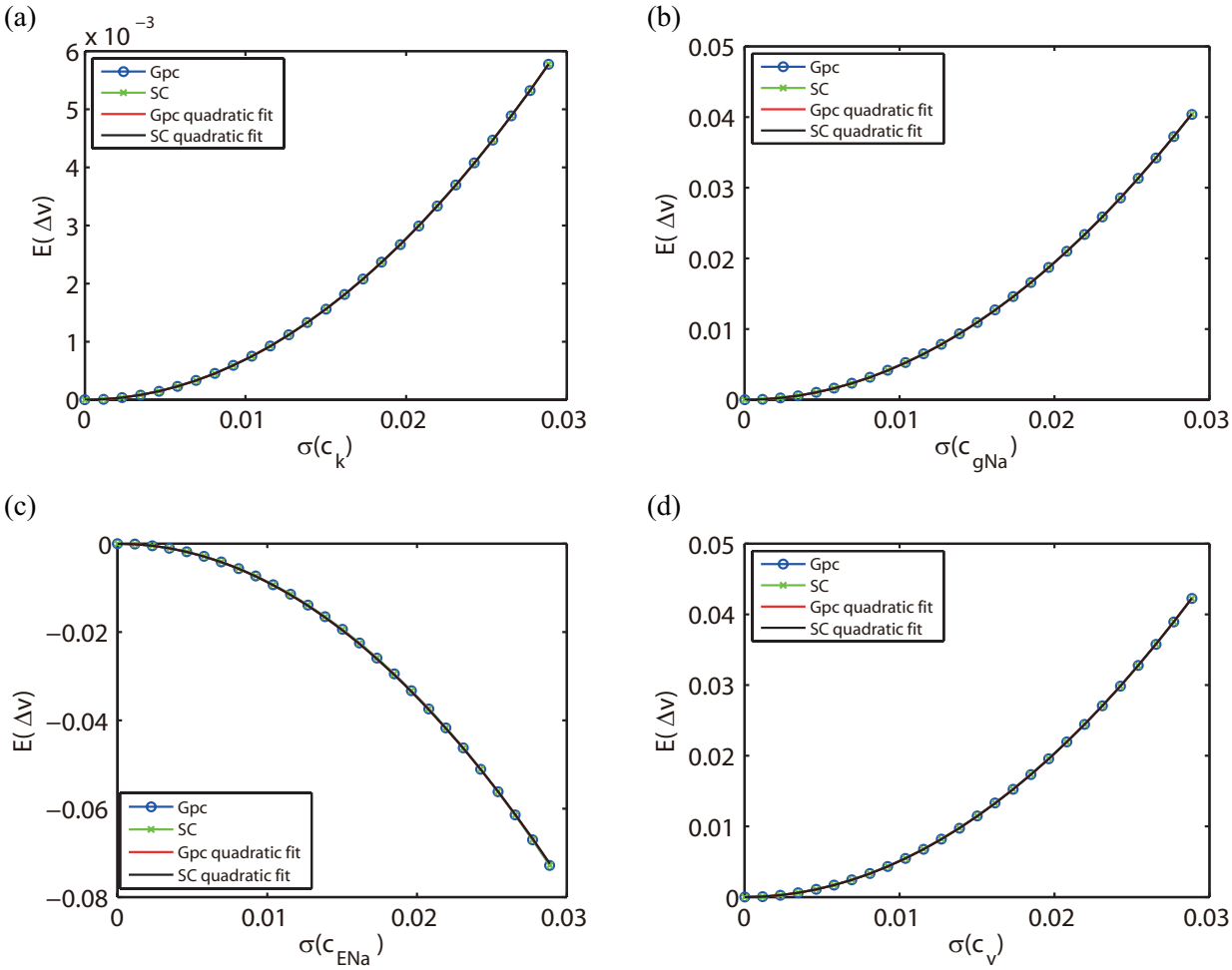

Figure 8: Observe the solution itself, *i.e.*, $\Delta Y_z = v(x,t;c_z) - v(x,t)$. Fix at a point $x = (0.5, 0.5)$ and in time $T = 3.0$. The blue lines are the numerical results of gPC and the red lines are the quadratically fitting lines; the green lines are the numerical results of SC and the black lines are quadratically fitting lines. (a): only k has a random perturbation; (b): only $\bar{g}_{\mathrm{Na}}$ has a random perturbation; (c): only E_{Na} has a random perturbation; (d): only $v(x,0)$ has a random perturbation;The quadratic relationship is shown.

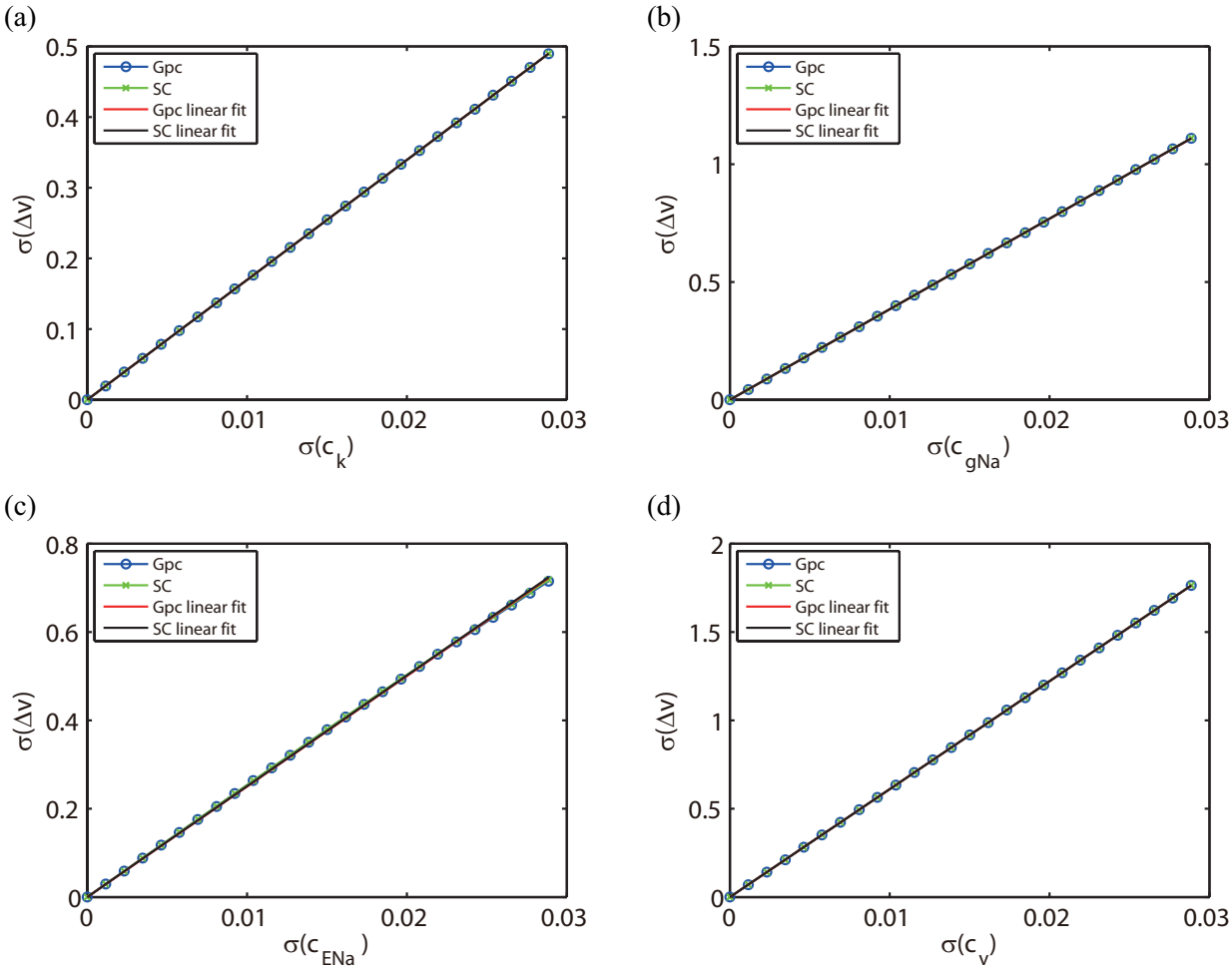

Figure 9: We observe the solution itself, *i.e.*, $\Delta Y_z = v(x,t;c_z) - v(x,t)$. Fix at a point $x = (0.5, 0.5)$ and in time $T = 3.0$. The blue lines are the numerical results of gPC and the red lines are the linearly fitting lines; the green lines are the numerical results of SC and the black lines are linearly fitting lines. (a): only k has a random perturbation; (b): only $\bar{g}_{\mathrm{Na}}$ has a random perturbation; (c): only E_{Na} has a random perturbation; (d): only $v(x,0)$ has a random perturbation; The linear relationship is shown.

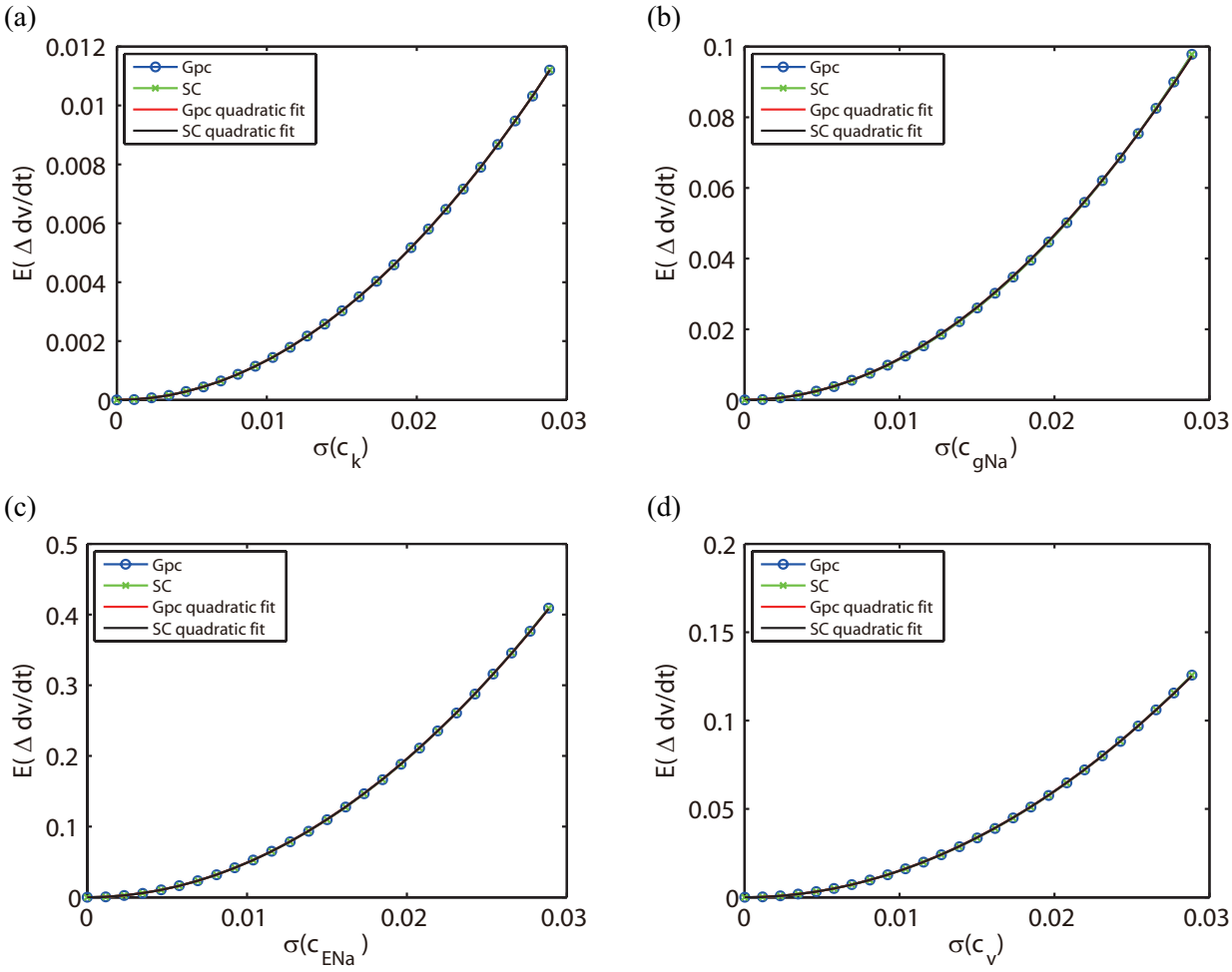

Figure 10: We observe the voltage derivative, *i.e.*, $\Delta Y_z = \dfrac{dv(x,t;c_z)}{dt} - \dfrac{dv(x,t)}{dt}$. Fix at a point $x = (0.5, 0.5)$ and in time $T = 3.0$. The blue lines are the numerical results of gPC and the red lines are the quadratically fitting lines; the green lines are the numerical results of SC and the black lines are quadratically fitting lines. (a): only k has a random perturbation; (b): only $\bar{g}_{\mathrm{Na}}$ has a random perturbation; (c): only E_{Na} has a random perturbation; (d): only $v(x,0)$ has a random perturbation; The quadratic relationship is shown.

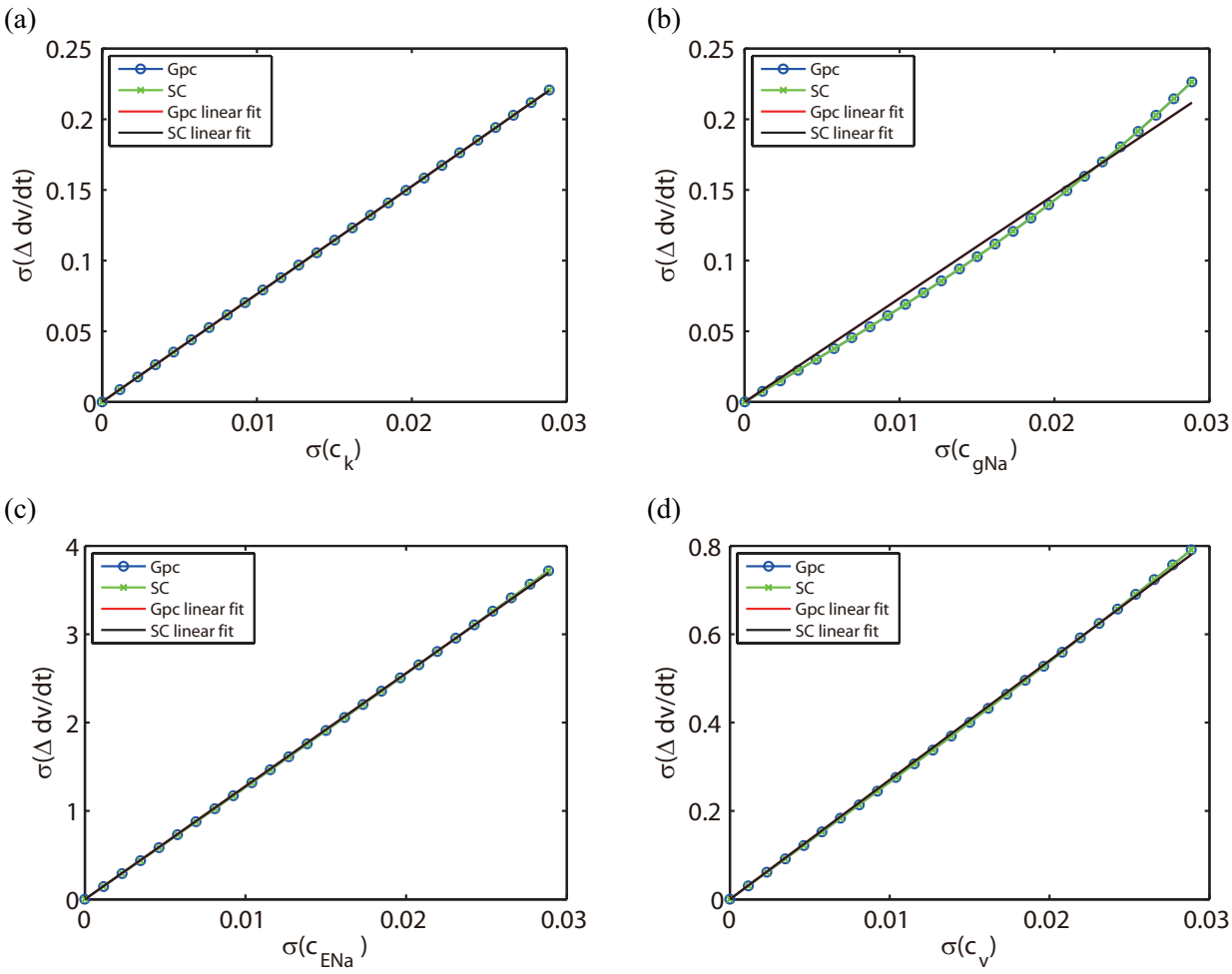

Figure 11: We observe the voltage derivative, *i.e.*, $\Delta Y_z = \dfrac{dv(x,t;c_z)}{dt} - \dfrac{dv(x,t)}{dt}$. Fix at a point $x = (0.5, 0.5)$ and in time $T = 3.0$. The blue lines are the numerical results of gPC and the red lines are the linearly fitting lines; the green lines are the numerical results of SC and the black lines are the linearly fitting lines. (a): only k has a random perturbation; (b): only $\bar{g}_{\mathrm{Na}}$ has a random perturbation; (c): only E_{Na} has a random perturbation; (d): only $v(x,0)$ has a random perturbation; The linear relationship is shown.